A New Type of Two-Dimensional Metal Coordination Systems: Hydrothermal Synthesis and Properties of the First Oxalate−bpy Mixed-Ligand Framework $^{2}_{\infty}$[M(ox)(bpy)] (M = Fe(II), Co(II), Ni(II), Zn(II); ox = $C_2O_4^{2-}$; bpy = 4,4′-bipyridine)

Jack Y. Lu, Michael A. Lawandy, and Jing Li*

Department of Chemistry, Rutgers University, Camden, New Jersey 08102

Tan Yuen and C. L. Lin

Department of Physics, Temple University, Philadelphia, Pennsylvania 19122

Received February 26, 1999

A new family of two-dimensional metal coordination polymers with the general formula $^{2}_{\infty}$[M(ox)(bpy)] (M = Fe(II), Co(II), Ni(II), Zn(II); ox = $C_2O_4^{2-}$; bpy = 4,4′-bipyridine) have been designed and synthesized via hydrothermal routes. Quantitative yields were obtained in all cases. The title compounds $^{2}_{\infty}$[Fe(ox)(bpy)] (**I**), $^{2}_{\infty}$[Co(ox)(bpy)] (**II**), $^{2}_{\infty}$[Ni(ox)(bpy)] (**III**), and $^{2}_{\infty}$[Zn(ox)(bpy)] (**IV**) represent the first coordination network structure constructed by bridging oxalate and 4,4′-bpy mixed ligands. **I**−**IV** are isostructural and belong to the orthorhombic crystal system, space group *Immm* (No. 71). The noninterpenetrated structure contains octahedral metal centers coordinated by two oxalate and two bpy ligands to form a two-dimensional layered network. Within each layer, relatively large rectangular voids are formed by four adjacent metal centers and the ligands bonded to them. The approximate dimensions of these cavities are 4 × 7 × 10 Å in the composite three-dimensional structures. Magnetic susceptibility and field-dependent magnetization measurements revealed spontaneous magnetic ordering with transition temperatures of 12, 13, and 26 K for **I**, **II**, and **III**, respectively. The types of ordering are interpreted as the antiferromagnetic kind with certain canting structures. The μ_{eff} values yielded from the fitting of $\chi(T)$ indicate the high spin states of M ions in all three compounds. The origin of the magnetic ordering in these compounds may be attributed to the strong exchange interactions between the M ions at the octahedral sites through the bridging oxalate molecules along the *a*-axis. Possible interchain coupling along the [011] direction is also considered. Thermogravimetric analysis studies indicate that all four compounds are thermally stable up to 290 °C (the on-set temperature of weight losses for **I**, 290 °C; **II**, 340 °C; **III**, 350 °C; and **IV**, 290 °C).

Introduction

Investigation of novel inorganic−organic hybrid framework assemblies represents one of the most active areas of materials science and chemical research. The intense interest in these materials is driven to a large extent by their interesting properties and potential in various applications, such as electrical conductivity,[1] magnetism,[2] photomechanism,[3] host−guest chemistry, ion exchange, shape specificity[4] and catalysis,[5,6] high-temperature, and flame-resistant fibers.[7] Incorporation of metal ions into organic systems often provides significant improvement to bulk properties such as thermal stability and dielectricity. The bonds formed in coordination polymers are usually stronger, more resistant to free-radical cleavage reactions, and exhibit higher thermal stability. Furthermore, metals often have variable valences, thus leading to a variety of frameworks to fulfill special needs. Many important properties of polymers depend largely on their structures and topology. Therefore, rational design and construction of new materials with specific networks have become a particularly important and topical subject.

Much effort has been made toward the synthesis of metal−organic coordination networks with the concept of rational design and crystal engineering.[8−10] The rational control of the formation of desired two-dimensional (2D) and three-dimen-

* To whom correspondence should be addressed. Fax: 609-225-6506. E-mail: jingli@crab.rutgers.edu.

(1) Manavalan, R.; Patel, M. M. *J. Makromol. Sci. Chem.* **1983**, *A19*, 951. Kobel, W.; Hanack, M. *Inorg. Chem.* **1986**, *25*, 103.
(2) Inoue, M.; Kubo, M. *Coord. Chem. Rev.* **1976**, *21*, 1. Kawata, S.; Kitagawa, S.; Kondo, M.; Furuchi, I.; Munakata, M. *Angew. Chem., Int. Ed. Engl.* **1994**, *33*, 1759.
(3) Jung, O.; Pierpont, C. G. *J. Am. Chem. Soc.* **1994**, *116*, 2229.
(4) Fujita, M.; Kwon, Y.; Washizu, S.; Ogura, K. *J. Am. Chem. Soc.* **1994**, *116*, 1151.
(5) Carlucci, L.; Ciani, G.; Proserpio, D. M.; Sironi, A. *J. Am. Chem. Soc.* **1995**, *117*, 4562.
(6) Robson, R.; Abrahams, B. F.; Batten, S. R.; Gable, R. W.; Hoskins, B. F.; Liu, J. *Supramolecular Architecture*; American Chemical Society: Washington, DC, 1992; Chapter 19. Hoskins, B. F.; Robson, R. *J. Am. Chem. Soc.* **1990**, *112*, 1546.
(7) van Krevelen, D. W. *Angew. Makromol. Chem.* **1972**, *22*, 133.
(8) See, for example, (a) Gable, R. W.; Hoskins, B. F.; Robson, R. *J. Chem. Soc., Chem. Commun.* **1990**, 1677. (b) Michaelides, A.; Kiritsts, V.; Skoulika, S.; Aubrey, A. *Angew. Chem., Int. Ed. Engl.* **1993**, *32*, 1495. (c) Aakeroy, C. B.; Seddon, K. R. *Chem. Soc. Rev.* **1993**, *22*, 397. (d) Parkinson, B. *Science* **1995**, *270*, 1157. (e) Fujita, M.; Kwon, Y.; Washizu, S.; Ogura, K. *J. Am. Chem. Soc.* **1994**, *116*, 1151. (f) Batten, S. R.; Robson, R. *Angew. Chem., Int. Ed. Engl.* **1998**, *37*, 1460.
(9) (a) Desiraju, G. R. *Crystal Engineering, The Design of Organic Solids*; Elsevier: Amsterdam, 1989. (b) MacGillivray, L. R.; Subramanian, S.; Zaworotko, M. J. *J. Chem. Soc., Chem. Commun.* **1994**, 1325. (c) Carlucci, L.; Ciani, G.; Proserpio, D. M.; Sironi, A. *J. Chem. Soc., Chem. Commun.* **1994**, 2755. (d) Subramanian, S.; Zawarotko, M. *Angew. Chem., Int. Ed. Engl.* **1995**, *34*, 2127. (e) Subramanian, S.; Zawarotko, M. *Coord. Chem. Rev.* **1994**, *137*, 357.

10.1021/ic990243w CCC: $18.00
Published on Web 05/06/1999

sional (3D) polymers are particularly important in the field of host−guest chemistry, ion exchange, shape-selective catalysis, and technology. The key to the construction of a desired framework is the selection of organic building blocks.[11]

The ability of bifunctional 4,4′-bipyridine (bpy) to act as a rigid, rodlike organic building block in the self-assembly of coordination frameworks is well-known.[8a,e,9b,c,10a,b,d] Much research has also been done on the metal oxalate ($C_2O_4^{2-}$) compounds, in the context of studies of molecular-based magnets and open framework structures.[12,13] The geometrical coordination mode and strength of this ligand provide both rigidity and preferred coordination specificity for metal centers.

Our recent efforts in designing new M^{2+}-based coordination network structures have focused largely on systems containing mixed multifunctional ligands. In this article, we describe the rational design and hydrothermal synthesis of a new family of two-dimensional divalent metal coordination frameworks $^2_\infty$[M(ox)(bpy)], M = Fe, Co, Ni, or Zn, as well as their magnetic and thermal properties.

Synthetic Rationale. A promising hydrothermal route[14] has been developed and applied to the synthesis of metal coordination networks.[15] Although the method is well-known for its ability to promote crystal growth and has been widely adopted in the preparation of many solid-state inorganic materials, it is relatively unexplored in the synthesis of coordination compounds.[10b,16] It has been shown that hydrothermal reactions often produce metastable compounds that may otherwise not be accessible by conventional methods. In our study, we have also learned that coordination compounds generated under supercritical conditions are often difficult to obtain by conventional solution synthesis.[15,17−20] One such example is the reductive cyclization of 2,2′-dipyradylamine(dpa) to give rise to dipyrido[1,2-a:2′,3′-d]imidazole in superheated water.[15a] Despite numerous studies that have been conducted on Cu/2,2′-dpa coordination systems, such a process has not been previously observed.

In an effort to synthesize mixed-ligand coordination systems containing both oxalate and 4,4′-bpy, we proposed a two-dimensional layered structure based on six-coordinate, divalent metal centers with a stoichiometric ratio of 1:1:1 for the metal, oxalate, and bpy. The $C_2O_4^{2-}$ ions are likely to link the metal centers from the opposite sides while the bipyridine ligands can readily approach the M^{2+} centers from both the top and the bottom, on the basis of their coordination habit and geometry considerations. The resultant 2D structure would contain metal centers with an octahedral coordination as shown in Scheme 1. One of the reasons for designing such a structure is to investigate possible magnetic interactions among the metal centers. Previous studies on an oxalato-bridging ligand has shown that it has a strong ability to mediate magnetic exchange interactions between metal ions more than 5 Å apart.[21] For the first-row transition metals, the distances between any two adjacent metal centers coordinated to a common oxalate ligand can be calculated and they are well within the vicinity of 5 Å. Incorporation of 4,4′-bpy ligands into the metal−oxalate chain structures may affect the magnetic ordering by introducing some interchain magnetic interactions. The proposed two-dimensional structure also contains rectangular-shaped voids, formed by four M^{2+} (corners of the rectangle), two $C_2O_4^{2-}$'s and two bpy's bonded to the metal centers (sides of the rectangle), which is by itself an interesting object to look into in terms of possible enclusion and enclathration activities. The proposed structure was accessed by hydrothermal reactions at 170 °C, which led to a family of four new compounds, $^2_\infty$[M(ox)(bpy)], M = Fe(II), Co(II), Ni(II), and Zn(II).

Scheme 1

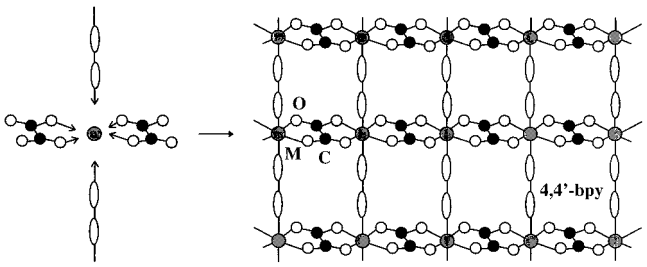

Experimental Section

Chemicals and Reagents. All chemicals used are as purchased without purification. $FeBr_2 \cdot 6H_2O$ (99.5%, Alfa Aesar), $CoCl_2$ (99.7%, Alfa Aesar), $CoBr_2 \cdot 6H_2O$ (99%, Alfa Aesar), $NiCl_2$ (99%, Alfa Aesar), $NiBr_2 \cdot 6H_2O$ (98%, Alfa Aesar), $ZnCl_2$ (98%, Aldrich), 4,4′-bypyridine (98%, Alfa Aesar), oxalic acid ($H_2C_2O_4 \cdot 2H_2O$, 97%, Alfa Aesar), and sodium oxalate ($Na_2C_2O_4$, 99%, Alfa Aesar).

Synthesis of $^2_\infty$[Fe(ox)(bpy)] (I). Crystals of **I** were isolated from reactions of $FeBr_2 \cdot 6H_2O$ (0.1618 g), bpy (0.0781 g), oxalic acid (0.063 g), and H_2O (4 mL) in the mole ratio of 1:1:1:444. The reactions were carried out in a 23 mL acid digestion bomb at 170 °C for 7 days. The product was washed with water and acetone and dried in air. Red plate crystals of **I** were collected in quantitative yield (0.15 g).

Synthesis of $^2_\infty$[Co(ox)(bpy)] (II). Reaction of $CoBr_2 \cdot 6H_2O$ (0.1638 g), bpy (0.0781 g), oxalate acid (0.0063 g), and H_2O (4 mL) in the mole ratio of 1:1:1:444 in a 23 mL acid digestion bomb at 170 °C for 7 days resulted in orange plate crystals in quantitative yield (0.15 g). Reactions using $CoCl_2$ (0.1298 g), bpy (0.1562 g), sodium oxalate (0.1340 g), and H_2O (8 mL) in the molar ratio of 1:1:1:444

(10) (a) Yaghi, O. M.; Li, G. *Angew. Chem., Int. Ed. Engl.* **1995**, *34*, 207. (b) Yaghi, O. M.; Li, H. *J. Am. Chem. Soc.* **1996**, *118*, 295. (c) Yaghi, O. M.; Li, H. *J. Am. Chem. Soc.* **1995**, *117*, 10401. (d) Yaghi, O. M.; Li, H.; Groy, T. L. *Inorg. Chem.* **1997**, *36*, 4292.

(11) Venkataraman, D.; Lee, S.; Zhang, J.; Moore, J. S. *Nature*, **1994**, *371*, 591.

(12) See, for example: (a) Decurtins, S.; Schmalle, H. W.; Schneuwly, P.; Zheng, L.-M.; Ensling, J.; Hauser, A. *Inorg. Chem.* **1995**, *34*, 5501. (b) Decurtins, S.; Schmalle, H. W.; Schneuwly, P.; Ensling, J.; Gutlich, P. *J. Am. Chem. Soc.* **1994**, *116*, 9521. (c) Decurtins, S.; Schmalle, H. W.; Schneuwly, P.; Oswald, H. R. *Inorg. Chem.* **1993**, *32*, 1888. (d) Decurtins, S.; Schmalle, H. W.; Oswald, H. R.; Linden, A.; Ensling, J.; Gutlich, P.; Hauser, A. *Inorg. Chim. Acta* **1994**, *216*, 65. (e) Tamaki, H.; Zhong, Z. J.; Matsumoto, N.; Kida, S.; Koikawa, M.; Achiwa, N.; Hashimoto, Y.; Okawa, H. *J. Am. Chem. Soc.* **1992**, *114*, 6979. (f) Curtis, N. F.; McCormick, I. R.; Waters, T. N. *J. Chem. Soc., Dalton Trans.* **1973**, 1537.

(13) (a) Speier, G.; Speier, E.; Noll, B.; Pierpont, C. G. *Inorg. Chem.* **1997**, *36*, 1520. (b) Glerup, J.; Goodson, P. A.; Hodgson, D. J.; Michaelsen, K. *Inorg. Chem.* **1995**, *34*, 6255.

(14) Ludise, R. A. In *Progress in Inorganic Chemistry*; Interscience Publishers: New York, 1962; Vol. 3. Rabenau, A. *Angew. Chem., Int. Ed. Engl.* **1985**, *24*, 1026. Laudise, R. A. *Chem. Eng. News* **1987** (Sept 28), 30.

(15) (a) Lu, J. Y.; Cabrera, B. R.; Wang, R.-J.; Li, J. *Inorg. Chem.* **1998**, *37*, 4480. (b) Lu, J. Y.; Cabrera, B. R.; Li, J. *Inorg. Chem.* Submitted.

(16) See, for example: Gutschke, S. O. H.; Slawin, A. M. Z.; Wood, P. T. *J. Chem. Soc., Chem. Commun.* **1995**, 2197. Yaghi, O. M.; Li, H. *J. Am. Chem. Soc.* **1996**, *117*, 10401. Gutschke, S. O. H.; Molinier, M.; Powell, A. K.; Winpenny, E. P.; Wood, P. T. *Chem. Commun.* **1996**, 823. Hagrman, D.; Hammond, R. P.; Haushalter, R.; Zubieta, J. *Chem. Mater.* **1998**, *10*, 2091.

(17) Cabrera, B. R.; Li, J.; Yuen, T. *Solid State Chemistry of Inorganic Materials II*, Mater. Res. Soc. Symp. Proc. Vol. 547; ISBN: 1-55899-453-X, 1999, p 493.

(18) Lawandy, M. A.; Wang, R.-J.; Li, J.; Yuen, T.; Lin, C. L. *Inorg. Chem.* Submitted.

(19) Pan, L.; Huang, X.-Y.; Li, J. *Chem. Commun.* Submitted.

(20) Wang, D.; Huang, X.-Y.; Li, J. *Chem. Mater.* Submitted.

(21) De Munno, G.; Ruiz, R.; Lloret, F.; Sessoli, R.; Julve, M. *Inorg. Chem.* **1995**, *34*, 408.

Table 1. Crystallographic Data for **I**, **II**, **III**, and **IV**

	I	**II**	**III**	**IV**
formula	$[Fe(C_2O_4)(N_2C_{10}H_8)]$	$[Co(C_2O_4)(N_2C_{10}H_8)]$	$[Ni(C_2O_4)(N_2C_{10}H_8)]$	$[Zn(C_2O_4)(N_2C_{10}H_8)]$
fw	300.05	303.13	302.91	309.57
space group	*Immm* (No. 71)	*Immm* (No. 71)	*Immm* (No. 71)	*Immm* (No. 71)
a, Å	5.476(1)	5.385(2)	5.303(1)	5.378(1)
b, Å	10.946(2)	10.945(2)	10.955(2)	10.967(2)
c, Å	11.471(2)	11.374(1)	11.257(2)	11.443(2)
V, Å^3	687.6(2)	670.4(2)	654.0(2)	674.9(2)
Z	2	2	2	2
ρ_{calc}, g cm^{-3}	1.449	1.502	1.538	1.523
μ, mm^{-1}	1.106	1.289	1.493	1.829
R [$I > 4\sigma(I)$]				
$R1^a$	0.044	0.026	0.024	0.040
w$R2^b$	0.103	0.065	0.059	0.092

[a] $R1 = (\sum||F_o| - |F_c|)/\sum|F_o|$. [b] $wR2 = (\sum[w(F_o^2 - F_c^2)^2]/\sum w(F_o^2)^2)^{1/2}$. $w = 1/[\sigma^2(F_o^2) + 55.02P]$; $P = (F_o^2 + 2F_c^2)/3$ for **I**. $w = 1/[\sigma^2(F_o2) + (0.0202P)^2 + 0.91p]$; $P = (F_o^2 + 2F_c2)/3$ for **II**. $w = 1/[\sigma^2(F_o^2) + (0.0081P)^2 + 0.60p]$; $P = (F_o^2 + 2F_c^2)/3$ for **III**. $w = 1/[\sigma^2(F_o^2) + (0.0402P)^2 + 1.91p]$; $P = (F_o^2 + 2F_c^2)/3$ for **IV**.

under identical experimental conditions gave a single phase of a polycrystalline sample of **II**.

Synthesis of $^2_\infty$[Ni(ox)(bpy)] (III). Light blue plate crystals of **III** were grown from a hydrothermal reaction containing $NiBr_2 \cdot 3H_2O$ (0.2665 g), bpy (0.1562 g), oxalate acid (0.1260 g), and H_2O (8 mL) in the mole ratio of 1:1:1:444. The same reaction conditions were applied as described for the crystal growth of **I** and **II**. The reaction again gave a quantitative yield (0.303 g). Single-phased powder samples of **III** were prepared by similar reactions of $NiCl_2$ (0.0.1296 g), bpy (0.1562 g), sodium oxalate (0.1340 g), and H_2O (8 or16 mL) with a mole ratio of 1:1:1:444 or 888.

Synthesis of $^2_\infty$[Zn(ox)(bpy)] (IV). Compound **IV** was synthesized in a manner similar to the one described above. Colorless transparent thin plates of **IV** were initially isolated from a reaction of $ZnCl_2$ (0.0682 g), bpy (0.0781 g), oxalate acid (0.0630 g), and H_2O (8 mL) in the mole ratio of 1:1:1:888. A yield of ~60% was calculated for this reaction. Polycrystalline, phase pure samples of **IV (**quantitative yield), were obtained from reactions of $ZnCl_2$ (0.1363 g), bpy (0.1562 g), sodium oxalate (0.1340 g), and H_2O (8 mL) in the mole ratio of 1:1:1:444.

Crystallographic Studies. A red plate crystal of **I** (0.2 × 0.3 × 0.5 mm), an orange plate crystal of **II** (0.1 × 0.2 × 0.5 mm), a light blue plate crystal of **III** (0.2 × 0.4 × 0.5 mm), and a colorless plate crystal of **IV** (0.02 × 0.02 × 0.1 mm) were selected for the crystal structure analysis. Each crystal was mounted on a glass fiber in air on an Enraf-Nonius CAD4 automated diffractometer. Twenty-five reflections were centered in each case using graphite-monochromated Mo Kα radiation. All data were collected at 295(2) K with the ω-scan method within the limits $7 \leq 2\theta \leq 50°$. Raw data were corrected for Lorentz and polarization effects, and an empirical absorption correction was applied in each case. The structures were solved using the SHELX-97 program.[22] The non-hydrogen atoms were located by direct phase determination and subjected to anisotropic refinement. The hydrogens were generated theoretically. The full-matrix least-squares calculations on F^2 were applied on the final refinements. The unit cell parameters, along with data collection and refinement details, are given in Table 1. Final atomic coordinates and average temperature factors are listed in Tables 2−5, and selected bond lengths and angles are reported in Tables 6−9. The structural factors and anisotropic displacement parameters are deposited as Supporting Information. Crystal drawings were generated by SCHAKAL 92.[23]

X-ray powder diffraction analyses were performed on a Rigaku D/M-2200T automated diffraction system (Ultima$^+$). All measurements were made between a 2θ range of 5 and 80° at the operating power of 40 kV/40 mA. All polycrystalline samples were examined for the purpose of phase identification.

(22) Sheldrick, G. M. *SHELX-97: program for structure refinement*; University of Goettingen: Germany, 1997.
(23) Keller, E. *SCHAKAL 92: a computer program for the graphical representation of crystallographic models*; University of Freiburg: Germany, 1992.

Table 2. Positional Parameters and U(eq)[a] for **I**

atom	*x*	*y*	*z*	*U*(eq)
Fe(1)	0.0000	0.5000	0.5000	0.0246(7)
O(1)	−0.2988(8)	0.6225(4)	0.5000	0.0307(12)
N(1)	0.0000	0.5000	0.3072(6)	0.035(2)
C(1)	−0.5000	0.5711(8)	0.5000	0.027(2)
C(2)	0.0000	0.3991(8)	0.2478(6)	0.073(3)
C(3)	0.0000	0.3952(8)	0.1269(6)	0.088(4)
C(4)	0.0000	0.5000	0.0652(8)	0.048(3)

[a] U(eq) is defined as one-third of the trace of the orthogonalized U_{ij} tensor.

Table 3. Positional Parameters and U(eq) for **II**

atom	*x*	*y*	*z*	*U*(eq)
Co(1)	0.0000	0.5000	0.5000	0.0199(3)
O(1)	−0.2936(3)	0.6230(16)	0.5000	0.0261(5)
N(1)	0.0000	0.5000	0.3113(3)	0.0304(8)
C(1)	−0.5000	0.5715(3)	0.5000	0.0210(9)
C(2)	0.0000	0.3987(4)	0.2500(3)	0.0688(14)
C(3)	0.0000	0.3947(3)	0.1291(3)	0.0757(16)
C(4)	0.0000	0.5000	0.0652(4)	0.0372(11)

Table 4. Positional Parameters and U(eq) for **III**

atom	*x*	*y*	*z*	*U*(eq)
Ni(1)	0.0000	0.5000	0.5000	0.0170(3)
O(1)	−0.2906(3)	0.6231(15)	0.5000	0.0221(5)
N(1)	0.0000	0.5000	0.3144(3)	0.0264(8)
C(1)	−0.5000	0.5715(3)	0.5000	0.0178(8)
C(2)	0.0000	0.3979(3)	0.2521(4)	0.0572(12)
C(3)	0.0000	0.3941(3)	0.1306(3)	0.0649(14)
C(4)	0.0000	0.5000	0.0651(4)	0.0343(11)

Table 5. Positional Parameters and U(eq) for **IV**

atom	*x*	*y*	*z*	*U*(eq)
Zn(1)	0.0000	0.5000	0.5000	0.0235(4)
O(1)	−0.2939(6)	0.6237(3)	0.5000	0.0285(8)
N(1)	0.0000	0.5000	0.3093(5)	0.0352(14)
C(1)	−0.5000	0.5721(5)	0.5000	0.0220(13)
C(2)	0.0000	0.3995(5)	0.2481(5)	0.076(3)
C(3)	0.0000	0.3948(5)	0.1289(5)	0.081(3)
C(4)	0.0000	0.5000	0.0640(6)	0.0409(18)

Thermal Analysis. Thermogravimetric analyses (TGA) of the title compounds were performed on a computer-controlled TA Instrument 2050TGA analyzer. Single-phased powder samples of **I** (9.4430 mg), **II** (5.4460 mg), **III** (11.0880 mg), and **IV** (28.1680 mg) were loaded into alumina pans and heated with a ramp rate of 10 °C/min from room temperature to 500−550 °C.

Magnetic Measurements. Magnetic measurements on polycrystalline samples of **I**, **II**, and **III** were performed using a Quantum Design SQUID magnetometer. These measurements include the field-dependent

Table 6. Bond Lengths [Å] and Angles [deg] for **I**[a]

Fe(1)−O(1)	2.116(4)	Fe(1)−N(1)	2.211(7)
O(1)−C(1)	1.237(6)		
O(1)−Fe(1)−O(1)	101.3(2)	O(1)−Fe(1)−O(1)	78.7(2)
O(1)−Fe(1)−O(1)	180.0	O(1)−Fe(1)−N(1)	90.0
N(1)−Fe(1)−N(1)	180.0		

[a] Symmetry transformations used to generate equivalent atoms: #1, −x, y, −z + 1; #2, x, −y + 1, z; #3, −x, −y + 1, −z + 1; #4, −x, −y + 1, z; #5, −x − 1, y, −z + 1; #6, −x − 1, −y + 1, −z + 1; #7, −x, −y + 1, −z.

Table 7. Bond Lengths [Å] and Angles [deg] for **II**

Co(1)−O(1)	2.0767(18)	Co(1)−N(1)	2.147(3)
O(1)−C(1)	1.246(2)		
2O(1)−Co(1)−O(1)	180.0	2O(1)−Co(1)−O(1)	80.83(10)
2O(1)−Co(1)−O(1)	99.17(10)	O(1)−Co(1)−N(1)	90.0
N(1)− Co(1)− N(1)	180.0		

Table 8. Bond Lengths [Å] and Angles [deg] for **III**

Ni(1)−O(1)	2.0477(18)	Ni(1)−N(1)	2.089(4)
O(1)−C(1)	1.246(2)		
2O(1)−Ni(1)−O(1)	97.63(9)	2O(1)−Ni(1)−O(1)	180.0
2O(1)−Ni(1)−O(1)	82.37(9)	O(1)−Ni(1)−N(1)	90.0
N(1)−Ni(1)−N(1)	180.0		

Table 9. Bond Lengths [Å] and Angles [deg] for **IV**

Zn(1)−O(1)	2.083(3)	Zn(1)−N(1)	2.182(5)
O(1)−C(1)	1.245(4)		
2O(1)−Zn(1)−O(1)	180.0	2O(1)−Zn(1)−O(1)	81.28(16)
2O(1)−Zn(1)−O(1)	98.72(16)	O(1)−Zn(1)−N(1)	90.0
N(1)−Zn(1)−N(1)	180.0		

magnetization $M(H)$ and magnetic susceptibility $\chi(T)$, defined as $M(T)/H$, where $M(T)$ is the temperature-dependent magnetization and H is the applied magnetic field. The temperature was varied in the $\chi(T)$ measurements from 2 to 350 K. Both the zero-field-cooled (ZFC) and field-cooled (FC) measurements were performed for each sample. $M(H)$ was measured at temperatures above and below the magnetic transition temperature for each sample. The applied magnetic field in $M(H)$ measurements was increased from 0 to 5.4 T and then decreased back to 0 T.

Results and Discussion

Synthesis. All reactions were carried out in 23 mL acid digestion bombs with Teflon liners. The overall reactions can be written as (A) when oxalic acid was used and (B) when the oxalate salt was used:

$$MX_2{\cdot}nH_2O + C_{10}H_8N_2 + H_2C_2O_4{\cdot}2H_2O \xrightarrow{H_2O} M(C_2O_4)(C_{10}H_8N_2) + 2HX + (n+2)H_2O \quad (A)$$

or

$$MX_2{\cdot}nH_2O + C_{10}H_8N_2 + Na_2C_2O_4 \xrightarrow{H_2O} M(C_2O_4)(C_{10}H_8N_2) + 2NaX + nH_2O \quad (B)$$

where M = Fe, Co, Ni, or Zn; X = Cl or Br.

In the case of (A), the solution pH values decreased from 5 to 3, indicating a significant increase in the acidity of the reaction media. Like in many other hydrothermal reactions, the crystallinity of the products was affected by the pH of the solution. In general, reactions of type A produced larger crystals, while reactions of type B gave mostly fine powder samples. Quantitative yields were obtained for all four compounds (**I**−**IV**).

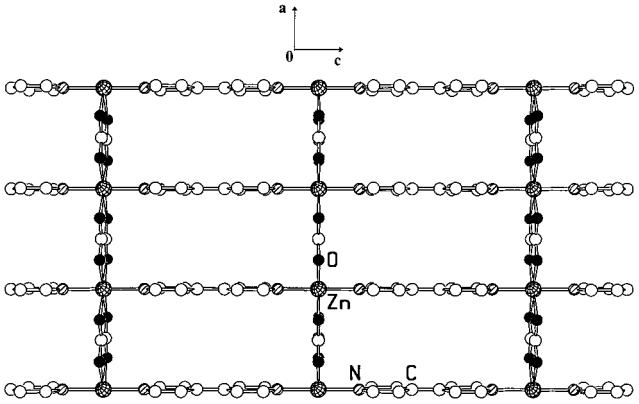

Figure 1. Two-dimensional network of $^2_\infty$[M(ox)(bpy)]. The cross-shaded circles are M (M = Fe, Co, Ni, Zn), open circles are C, solid circles are O and shaded circles are N.

The hydrothermal conditions were crucial for the formation and crystallization of the title compounds. Solution synthesis using zinc chloride ($ZnCl_2$), oxalic acid, and 4,4′-bipyridine in the same medium (H_2O) afforded polycrystalline $Zn(C_2O_4)\cdot 2H_2O$ in high yield. Powder X-ray diffraction analysis confirmed that the sample does not contain **IV**. Variation in solvents (acetone and ethanol) while keeping other experimental conditions such as reaction temperature and composition unchanged led to different products.

Structures. Compounds **I**, **II**, **III**, and **IV** crystallize in the orthorhombic crystal system, space group *Immm* (No. 71). The unit cell parameters are $a = 5.476(1)$, $b = 10.946(2)$, and $c = 11.471(2)$ Å for **I**; $a = 5.385(1)$, $b = 10.945(2)$, and $c = 11.374(2)$ Å for **II**; $a = 5.378(1)$, $b = 10.967(2)$, and $c = 11.443(2)$ Å for **III**; $a = 5.303(1)$, $b = 10.955(2)$, and $c = 11.257(2)$ Å for **IV**, respectively. The crystal structure consists of two-dimensional $^2_\infty[M(C_2O_4)(C_{10}H_8N_2)]$ networks (Figure 1). All metal atoms (M = Fe, Co, Ni, Zn) are divalent and have an octahedral coordination with four oxygen atoms from oxalate ions ($C_2O_4^{2-}$) and two nitrogen atoms from bipyridine molecules. The 2D sheets so-formed contain large rectangular-shaped voids (cross section $\sim a \times c$), enclosed by four M^{2+} located at the four corners of the rectangle, two $C_2O_4^{2-}$'s and two bpy's, each bridging to two metal centers. It is not difficult to understand why these two-dimensional nets do not interpenetrate to form an interlocked structure, since the open space along the a direction is too small to accommodate another net. Instead, these 2D nets stack on top of each other in a staggered fashion (the adjacent layers are shifted by $^1/_2a + {}^1/_2c$) to complete the structure in the third dimension (Figure 2). The distance between any two adjacent layers is $^1/_2b$ (approximately 5.5 Å). The resultant structure contains "voids" that may be conceptually enclosed by six adjacent metal centers and the ligands bonded to them: four in the middle layer with two oxalate anions and two bipyridyl groups, one in the top and the other in the bottom layer. The approximate dimensions of these voids are 4 × 7 × 10 Å based on the covalent volumes and are roughly 2 × 5 × 8 Å based on the van der Waals volumes.

The M−O distances (Fe−O, 2.116(4) Å; Co−O, 2.077(2) Å; Ni−O, 2.048(2) Å) are comparable to those found in oxalato complexes (Fe−O, 1.962(2)−2.039(2) Å; Ni−O, 2.10(2)−2.13(1) Å),[12c,24a] and with each other. The Zn−O distance, 2.083(3) Å, is similar to those in a one-dimensionl (1D) chain compound $^1_\infty$[(ox)Zn(dpa)], in which the Zn−O distances range from 2.074(2) to 2.108(2) Å.[20] The M−N distances (Fe−N, 2.211(7) Å; Co−N, 2.147(3) Å, and Ni−N, 2.089(4)

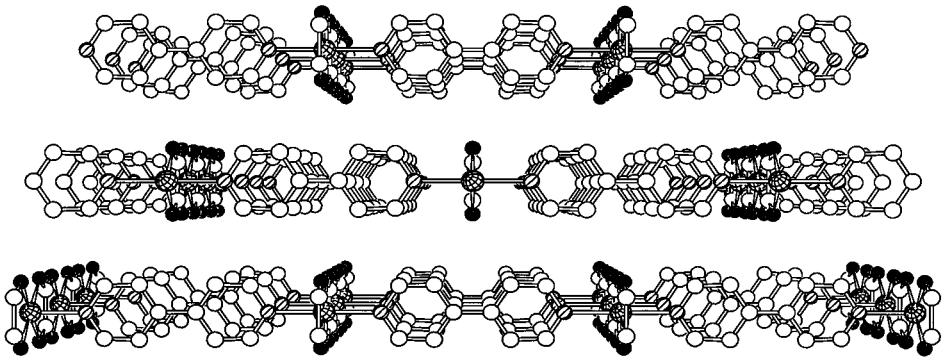

Figure 2. Perspective view of the structure. The $^{2}_{\infty}$[M(ox)(bpy)] 2D layers are stacked in a staggered fashion along the *b* axis. The labeling scheme is the same as that defined in Figure 1.

Å) are also comparable to those reported (Co−N, 1.926(8)−2.114(8) Å; Ni−N, 2.08(1)−2.149(2) Å).[10d,24b] The Zn−N distance (2.182(5) Å) is slightly longer than those found in several other zinc−bpy compounds.[8a,9d,16] All O−M−N and N−M−N angles are precisely 90° and 180°, respectively.

The M−M distances within the 2D net are *a* (5.3−5.5 Å) and *c* (11.3−11.5 Å), respectively. While the distances along the *c* direction are too long for any significant magnetic interactions, it is anticipated that relatively strong magnetic exchange interactions along the *a* direction are likely to be observed for the Fe, Co, and Ni phases. The detailed discussions regarding these interactions will be given in the section that follows.

Coordination polymers containing infinite M-(4,4′-bpy) network structures are quite common. Several recently reported systems include noninterpenetrating one-dimensional [Ni(4,4′-bpy)$_{2.5}$(H$_2$O)$_2$(ClO$_4$)$_2$]·1.5(4,4′-bpy)·2H$_6$O,[10d] Co(SO$_4$)(H$_2$O)$_3$-(4,4′-bpy)·2H$_2$O,[24c] and Co(NCS)$_2$(H$_2$O)$_2$(4,4′-bpy)·(4,4′-bpy);[24d] two-dimensional square networks of [Cd(4,4′-bpy)$_2$(NO$_3$)$_2$]·(C$_6$H$_4$Br$_2$)$_2$[4] and [M(4,4′-bpy)$_2$(H$_2$O)$_2$](ClO$_4$)$_4$·(CLA),[24e] M = Cu, Zn, Cd, of CLA = enclathrated molecules; three-dimensional Zn(4,4′-bpy)$_2$(SiF$_6$)]·*x*DMF;[9d] and three-dimensional interpenetrating [Zn(4,4′-bpy)$_2$(H$_2$O)$_2$]·SiF$_6$.[9d] A number of coordination polymers containing single or mixed oxalate ligands have also been synthesized. These include one-dimensional [Cu(en)$_2$][Cu(ox)$_2$],[25] [Cu(ox)(2,2′-bpy)]·2H$_2$O,[25] and [Cu$_2$(ox)$_2$(μ-pyz)(pyz)],[26] two-dimensional [Cu$_2$(ox)(bpym)-Cl$_2$][12a] and [Mn$_2$(ox)(bpm)]·2H$_2$O,[21] and three-dimensional [Fe(2,2′-bpy)$_3$] [Fe$_2$(ox)$_3$].[12c] It is, however, somewhat surprising that simple, infinite networks of metal oxalate−bpy mixed ligand systems have not been investigated prior to this study. Our literature search shows that the only oxalate/4,4′-bpy coordination compounds reported thus far include a discrete Ru$_4$ cluster compound[27] and a molecular mononuclear Cr compound.[28] Although [NaCr(ox)$_2$(bpy)(H$_2$O)]·2H$_2$O[28] is a two-dimensional structure, the 4,4′-bpy acts as a terminal ligand in this compound and does not contribute to the construction of the 2D network. The title compounds represent a new type of 2D neutral octahedral coordination polymers.[29]

Magnetic Properties. The magnetic susceptibility data, $\chi(T) = M(T)/H$, for **I**, **II**, and **III** are shown in Figures 3−5, respectively. A magnetic field of 0.1 T was applied in all these measurements. In addition, $\chi(T)$ was measured for **I** under 0.5 T. We will not show the $\chi(T$, 0.5 T) curve separately since its shape is essentially the same as $\chi(T$, 0.1 T). For **II**, we also measured $\chi(T)$ under 0.01 T. The shape of $\chi(T$, 0.01 T) (not shown) is similar to that of $\chi(T$, 0.1 T), except that the zero-field-cooled data decreases as T decreases below 8 K. The anomalies seen in the low-temperature region of each $\chi(T)$ data set indicate that there exists a spontaneous magnetic ordering below a transition temperature in each of the three compounds. Above the transition temperatures, the $\chi(T)$ data were fit to a modified Curie−Weiss law, $\chi(T) = \chi_0 + C/(T + \theta)$. We plot $1/[\chi(T) - \chi_0]$ as a function of T in the inserts of Figures 3−5. The fitting parameters, including temperature-independent magnetic susceptibility, χ_0, effective magnetic moment, $\mu_{\text{eff}} = 2.83(C)^{1/2}$, and the Curie−Weiss temperature, θ, are listed in Table 10. The values of μ_{eff} yielded from the fitting indicate a high spin state for each M(II) ion. Although the $\chi(T)$ data suggest a ferromagnetic ordering for **I** and **II**, and a simple antiferromagnetic ordering for **III**, the ground-state magnetic structures for these compounds are more complicated, as we shall discuss in later paragraphs. Nonetheless, we claim that the magnetic orderings in all these compounds exhibit a certain antiferromagnetic nature. These interpretations are consistent with the fact that the fitting parameters for the Curie−Weiss temperature θ are negative for all three compounds. In Table 10, we also list the antiferromagnetic transition temperature denoted as T_N, at which the $\chi(T)$ anomalies are observed. The origin of the anomaly around $T = 250$ K seen in $\chi(T)$ versus T of Figure 3 is unclear to us at this time, and the fitting was exclusive of the $\chi(T)$ data above 240 K.

Shown in Figure 6 is the field-dependent magnetization, $M(H)$, measured at 2 K for **I**. No hysteresis was found in $M(H)$ measurements of this compound as well as the other two compounds. The linear and nonsaturating behavior of the $M(H)$ at $H > 1.5$ T strongly suggests an antiferromagnetic state of the sample at this temperature. Yet the curved $M(H)$ in the $H < 1.5$ T region with decreasing slope clearly shows a contribution to $M(H)$ from a ferromagnetic component. In fact, such a behavior of $M(H)$ is typical for a canted antiferromagnetic

(24) (a) Roman, P.; Guzman-Miralles, C.; Luque, A.; Beitia, J. I.; Cano, J.; Lloret, F.; Julve, M.; Alvarez, S. *Inorg. Chem.* **1996**, *35*, 3741. (b) Faus, J.; Julve, M.; Lloret, F.; Real, J. A.; Sletten, J. *Inorg. Chem.* **1994**, *33*, 5535. (c) Lu, J.; Yu, C.; Niu, T.; Paliwala, T.; Crisci, G.; Somosa, F.; Jacobson, A. J. *Inorg. Chem.* **1998**, *37*, 4637. (d) Lu, J.; Paliwala, T.; Lim, S. C.; Yu, C.; Niu, T.; Jacobson, A. J. *Inorg. Chem.* **1997**, *36*, 923. (e) Tong, M.-L.; Ye, B.-H.; Cai, J.-W.; Chen, X.-M.; Ng, S. W. *Inorg. Chem.* **1998**, *37*, 2645.
(25) Oshio, H.; Nagashima, U. *Inorg. Chem.* **1992**, *31*, 3295.
(26) Kitagawa, S.; Okubo, T.; Kawata, S.; Kondo, M.; Katada, M.; Kobayashi, H. *Inorg. Chem.* **1995**, *34*, 4790.
(27) Yan, H.; Suss-Fink, G.; Neels, A.; Stoeckli-Evans, H. *J. Chem. Soc., Dalton Trans.* **1997**, 4345.
(28) Muñoz, M. C.; Julve, M.; Lloret, F.; Faus, J.; Andruh, M. *J. Chem. Soc., Dalton Trans.* **1998**, 3125.

(29) An "octahedral polymer" was defined in ref 9d as an infinite 3D framework that is sustained by octahedral metal centers cross-linked by linear bifunctional ligands. Here, we extend this definition to include all 1D, 2D, and 3D extended networks (octahedral metal centers).

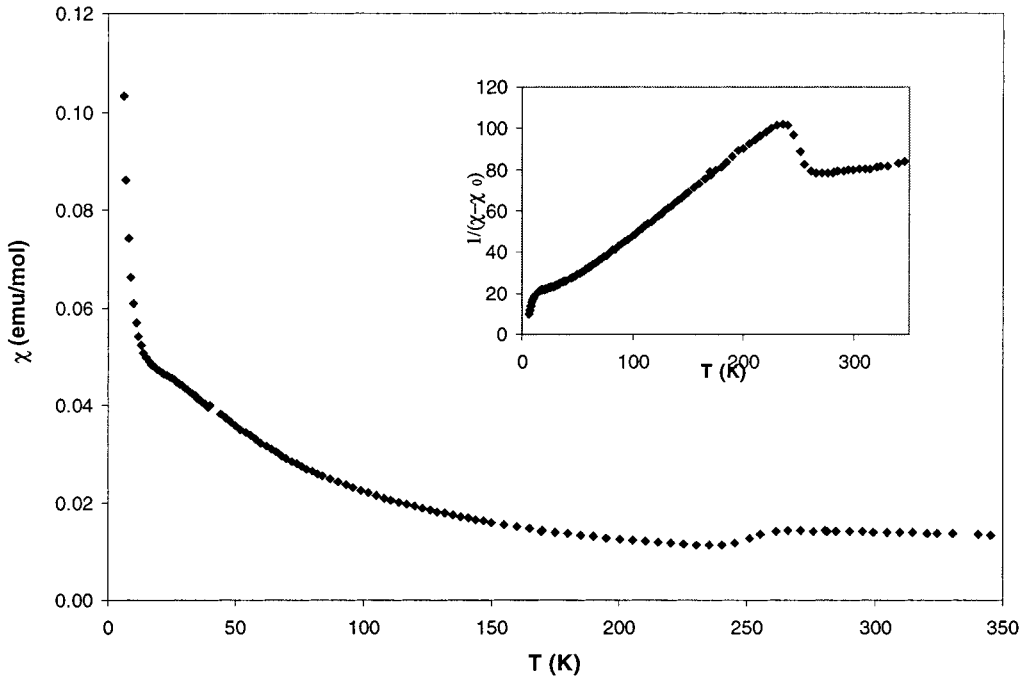

Figure 3. Temperature-dependent susceptibility $\chi(T)$ data measured in an applied field of 0.1 T on a polycrystalline sample of **I**. Inserted is a plot of $1/[\chi(T) - \chi_0]$ vs T (K).

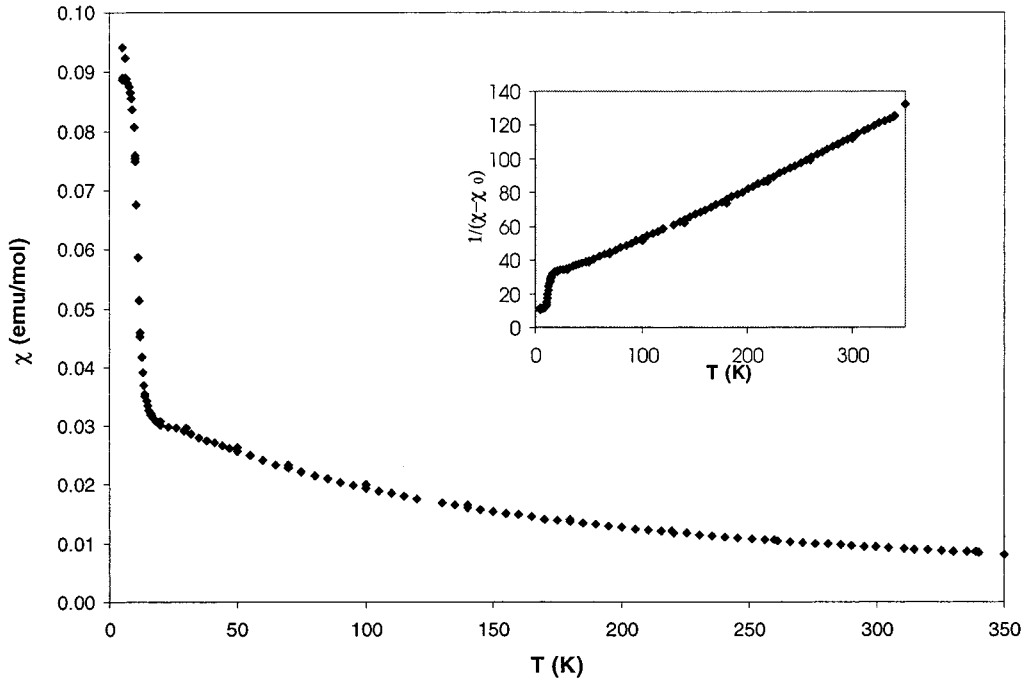

Figure 4. $\chi(T)$ data measured in an applied field of 0.1 T on a polycrystalline sample of **II**. Inserted is a plot of $1/[\chi(T) - \chi_0]$ vs T.

ordering. The resulting nonzero magnetic moment in a particular direction from such an ordering is also the cause of the anomaly seen in the $\chi(T)$ data as being apparently ferromagnetic alike. $M(H)$ measurements on compound **II** were performed at 4.5 K and at 11−18 K, with a 1 K increment of temperature. In Figure 7 we show the $M(H)$ data at 4.5, 11, and 18 K. Using the same argument for interpreting the low-temperature $M(H)$ data for **I**, we can interpret the $M(H,$ 4.5 K) data as due to a similar canted antiferromagnetic ordering. More interestingly, we noticed the evolution of the $M(H)$ from the temperature region below T_N, around T_N, and above T_N. Comparing the data of $M(H,$ 11 K) and $M(H,$ 18 K) to $M(H,$ 4.5 K), we can see that as T increases near T_N, the slope of the high field part in $M(H,$ 11 K) increases, while the ferromagnetic contribution in the low field part decreases. As T is increased above T_N, $M(H,$ 18 K) becomes paramagnetic-like and the slope of the $M(H,$ 18 K) becomes even larger. Furthermore, the three $M(H)$ curves intersect at H around 1 T. This indicates that, under a stronger field than 1 T, the canting of the Co moments will be changed, resulting in a more antiferromagnetically ordered state. Indeed, we can predict that if measured under $H > 1$ T, $\chi(T)$ will look like a typical antiferromagnet in that $\chi(T)$ will decrease with decreasing T below T_N. In Figure 8 we present the $M(H)$ data measured at 2 and 30 K for **III**. One may expect a rather simple $M(H)$ behavior because of a very typical antiferromagnetic-like $\chi(T)$, as shown in Figure 5. However, an upturn around $H = 4.8$ T in the $M(H,$

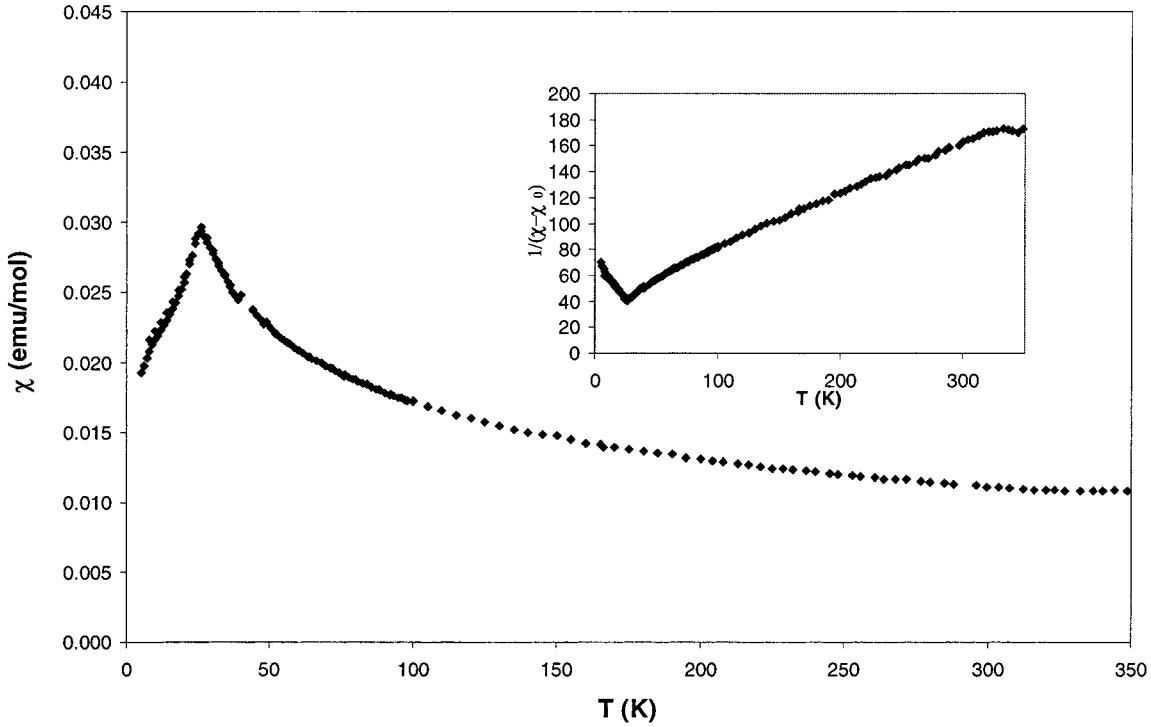

Figure 5. $\chi(T)$ data measured with an applied field of 0.1 T on a polycrystalline sample of **III**. Inserted is a plot of $1/[\chi(T) - \chi_0]$ vs T.

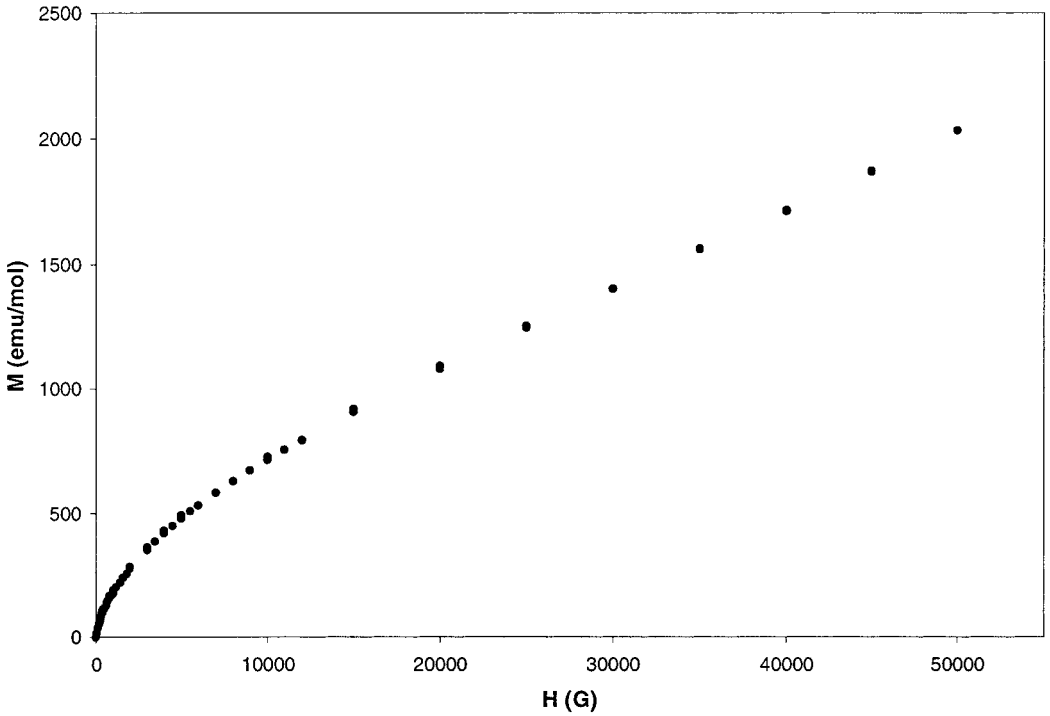

Figure 6. $M(H)$ measured at 2 K on a powder sample of **I**. The applied magnetic field was increased from 0 to 5.4 T and then decreased back to 0 T. No hysteresis was observed.

Table 10. Fitting Parameters in χ(T) for **I**, **II**, and **III**

compd	χ_0 (emu/mol)	μ_{eff} (μ_B)	θ (K)	T_N (K)
Fe(ox)(bpy), **I**	1.5×10^{-3}	4.71	−33	12
Co(ox)(bpy), **II**	5.5×10^{-4}	5.45	−98	13
Ni(ox)(bpy), **III**	5.0×10^{-3}	4.33	−89	26

2 K) curve was observed. This slope change in $M(H)$ suggests that the ground-state magnetic ordering is again a canted antiferromagnet. Below T_N and under a field $H > 5$ T, the magnetic moments of the Ni in the compound are anticipated to reorient themselves to other directions, resulting in a larger contribution in $M(H)$.

The interesting magnetic properties in the M(ox)(bpy) series are originated from the strong M−M exchange interaction through extended oxalate bridges. As seen in Figures 1 and 2, the magnetic M ions at the octahedral sites form chains with intrachain separation of 5.303−5.476 Å. Although the M−M separation is quite large, the bonding between the oxalates and the M ion makes the transmission of the M−M magnetic coupling very effective. Since the M−M interchain separations in [010] and [001] directions are in the vicinity of 11 Å, we may neglect any possible M−M interchain coupling in these two directions. However, the M−M interchain separation in the

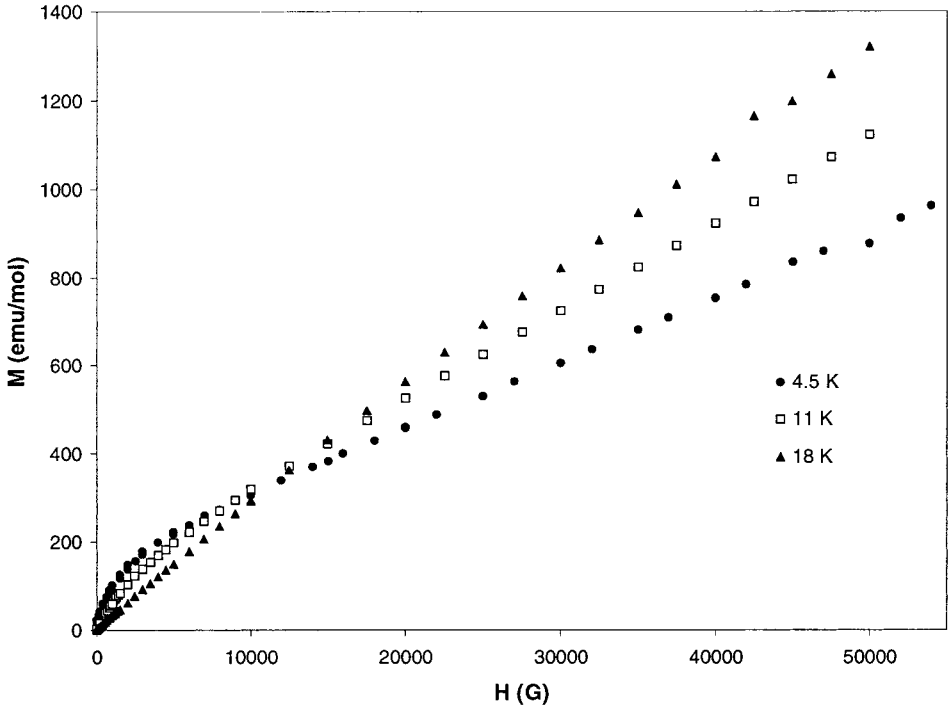

Figure 7. *M*(*H*) measured at 4.5, 11, and 18 K on powder samples of **II**. The applied magnetic field was increased from 0 to 5.4 T and then decreased back to 0 T for every measurement. No hysteresis was observed.

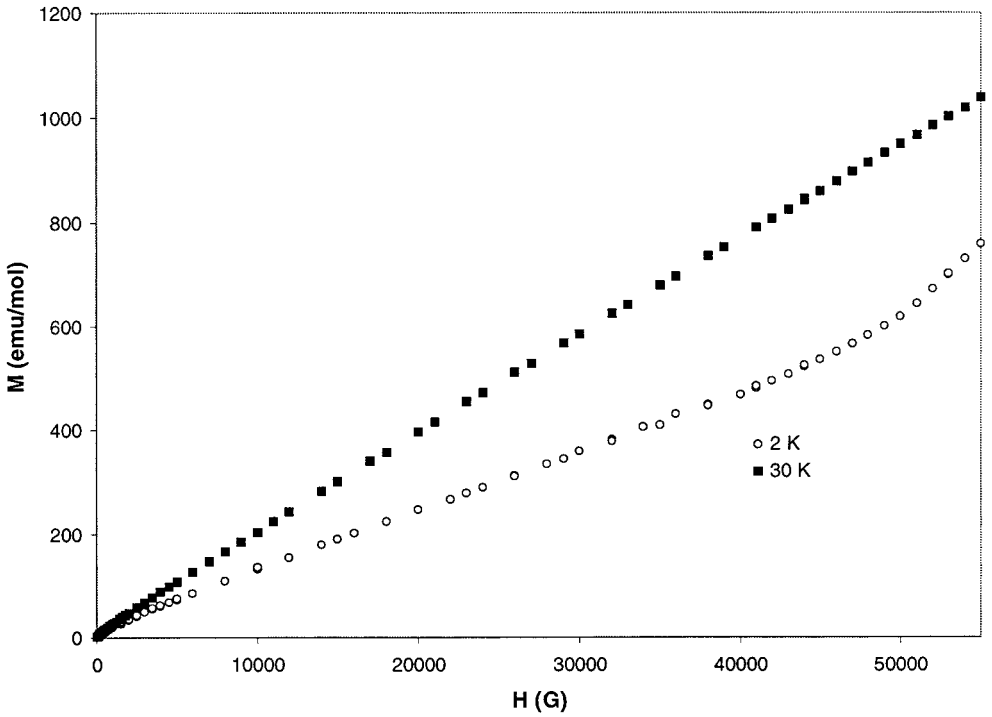

Figure 8. *M*(*H*) measured at 2 and 30 K on powder samples of **III**. The applied magnetic field was increased from 0 to 5.4 T and then decreased back to 0 T for each measurement. No hysteresis was observed.

[111] direction ranges from 8.290 to 8.387 Å, suggesting a possible M−M coupling along this direction, which complicates the ground-state magnetic structure. Although the spontaneous orderings at low temperatures found in these compounds are all antiferromagnetic in nature, as we have discussed above, the subtle differences in the magnetic behavior of the three compounds observed are nonetheless dictated by the differences in the electronic structures of the M ions.

Thermal Stability. Plotted in Figures 9−12 are the results from thermogravimetric analyses performed on **I**−**IV**. The weight losses observed for all four compounds along with the negative values of the first derivatives (%/°C) are shown as functions of temperature between 50 and 500 °C. These curves clearly indicate that all four compounds are quite robust. They underwent a single-step weight loss process and are thermally stable up to at least 290 °C. The on-set temperatures of the weight losses are approximately 290 °C for **I**, 340 °C for **II**, 350 °C for **III**, and 290 °C for **IV**. The decomposition process completed at approximately 460 °C for **I**, 490 °C for **II**, 530 °C for **III**, and 430 °C for **IV**. The demonstrated thermal stability

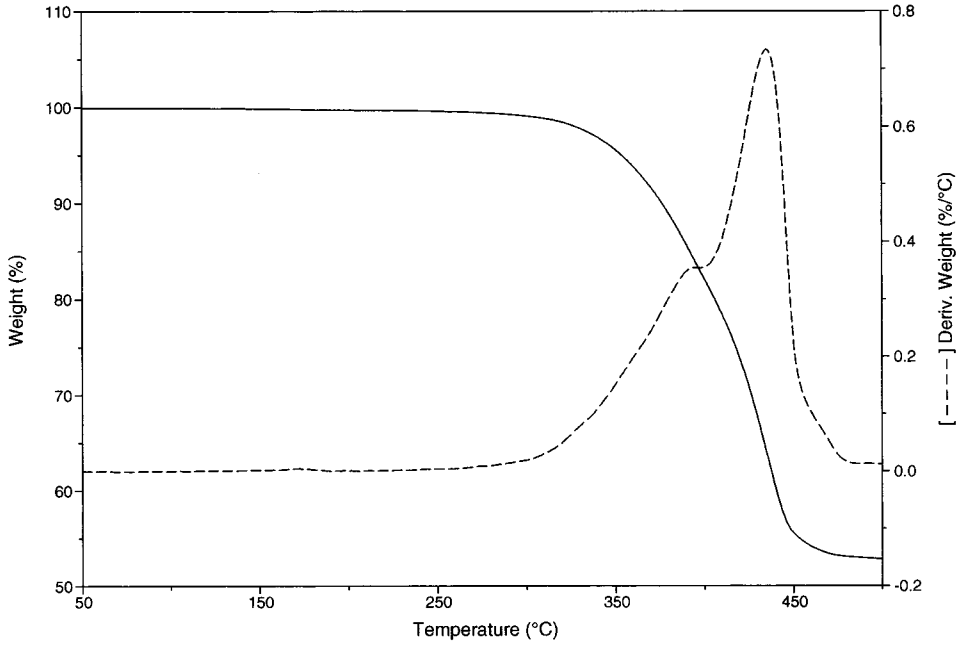

Figure 9. Thermogravimetric analysis (TGA) data showing weight loss of **I** (solid line) between 50 and 500 °C. The negative of the first derivative (%/°C, dashed line) is also plotted as a function of temperature.

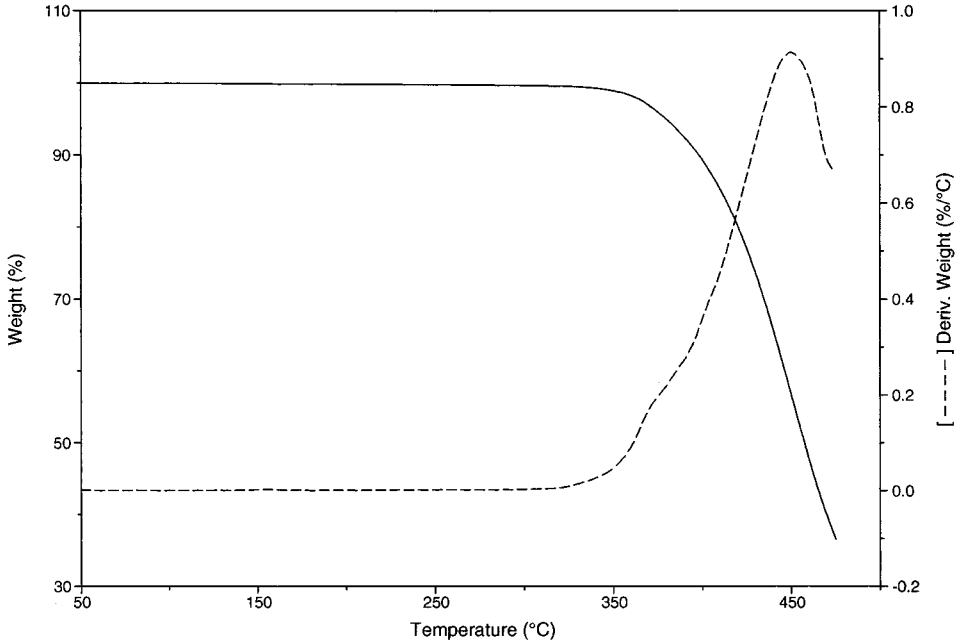

Figure 10. Thermogravimetric analysis (TGA) data showing weight loss of **II** (solid line) between 50 and 500 °C. The negative of the first derivative (%/°C, dashed line) is also plotted as a function of temperature.

of these compounds could be, at least partially, attributed to the weak $\pi-\pi$ interactions between the bpy rings from the adjacent units along the *a*-axis. All bpy rings are perpendicular to the *ac*-planes so that they are parallel to each other. The distance between any two adjacent rings is the unit cell length of *a* (5.3−5.5 Å) which is subject to a weak $\pi-\pi$ interaction that stabilizes the structure. The chelating nature of the oxalate ligand may also enhance the stability of the structure. The weight loss curves clearly indicate that no water molecules are incorporated in any of these compounds through inclusion. The same situation has been noticed in the hydrothermal synthesis of other compounds under the similar experimental conditions.[15b,18]

Concluding Remarks

A new family of two-dimensional coordination compounds containing mixed oxalate−bpy ligands have been designed and synthesized in high yields via hydrothermal routes. All four compounds are relatively stable, due likely to the weak $\pi-\pi$ interactions between the adjacent (parallel) bipyridine rings and to the enhanced structural stability by chelating oxalate ligands. The designing of this layered structure and incorporation of magnetic metal centers into such a structure (**I**−**III**) enables the formation of a one-dimensional magnetic chain coupled with weak interchain interactions which results in antiferromagnetic ordering with some canting features. The ground-state magnetic structures in these systems are quite complex which offers an

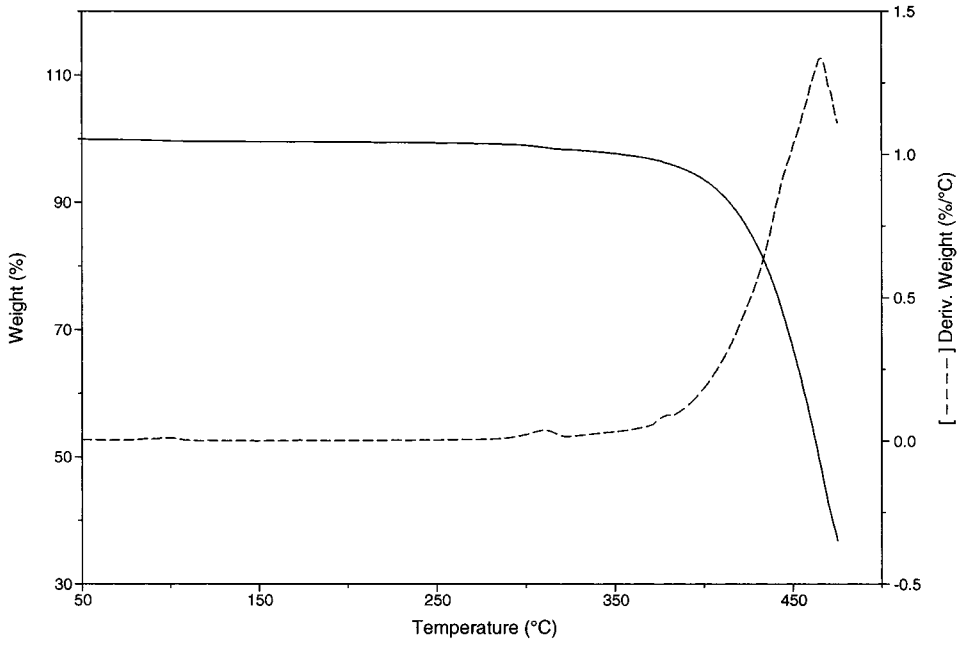

Figure 11. Thermogravimetric analysis (TGA) data showing weight loss of **III** (solid line) between 50 and 500 °C. The negative of the first derivative (%/°C, dashed line) is also plotted as a function of temperature.

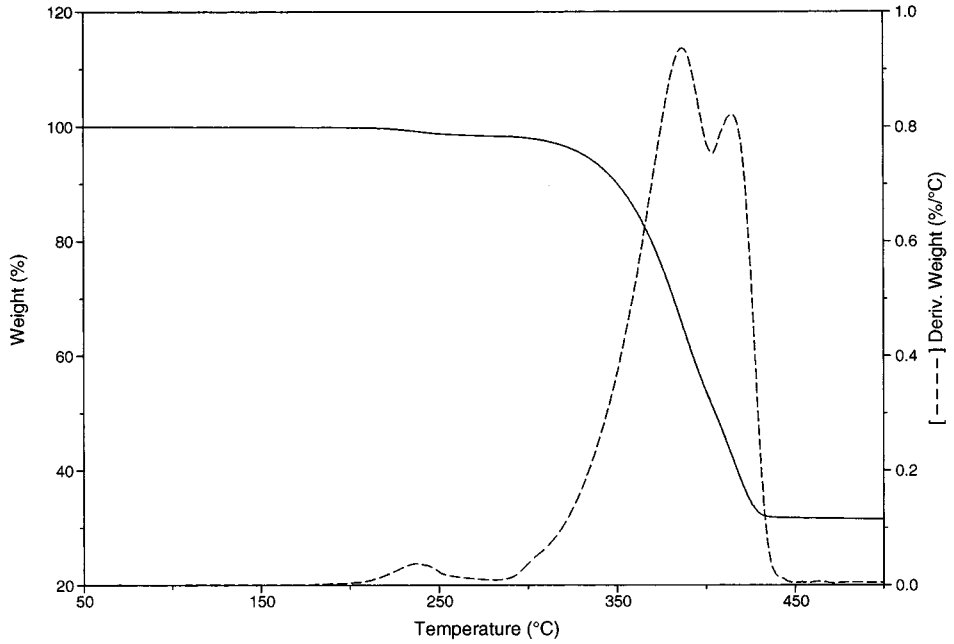

Figure 12. Thermogravimetric analysis (TGA) data showing weight loss of **IV** (solid line) between 50 and 500 °C. The negative of the first derivative (%/°C, dashed line) is also plotted as a function of temperature.

excellent topic for further systematic experimental and theoretical investigations.

Acknowledgment. Financial support from the National Science Foundation (DMR-9553066 and DMR-9633018) is greatly appreciated. J.L. would like to thank Professor Jon Clardy and Professor Roald Hoffmann for their enlightening comments and suggestions. The FT-IR/TGA/DSC apparatus was purchased through a NSF ARI grant (CHE 9601710-ARI).

Supporting Information Available: Tables of crystallographic data, atomic coordinates, isotropic and anisotropic thermal parameters, bond distances and angles for compounds **I**−**IV**, and a plot of the asymmetric unit in **I** showing 50% thermal vibration ellipsoids. Ordering information and instructions for Internet access is given on any current masthead page.

IC990243W